Acta Oceanol. Sin., 2021, Vol. 40, No. 7, P. 88–99
https://doi.org/10.1007/s13131-021-1739-9
http://www.aosocean.com
E-mail: ocean2@hyxb.org.cn

Seasonal variation in the three-dimensional structures of coastal thermal front off western Guangdong

Yan Zhang[1, 3], Lili Zeng[2], Qiang Wang[2], Bingxu Geng[2], Changjian Liu[1, 3], Rui Shi[2], Na Liu[2], Weiping Wang[1, 3*], Dongxiao Wang[2]

[1] South China Sea Marine Survey and Technology Center, Ministry of Natural Resources, Guangzhou 510300, China

[2] State Key Laboratory of Tropical Oceanography (LTO), South China Sea Institute of Oceanology, Chinese Academy of Sciences, Guangzhou 510301, China

[3] Key Laboratory of Marine Environmental Survey Technology and Application, Ministry of Natural Resources, Guangzhou 510300, China

Received 17 July 2020; accepted 17 September 2020

© Chinese Society for Oceanography and Springer-Verlag GmbH Germany, part of Springer Nature 2021

Abstract

The seasonal structure and dynamic mechanism of oceanic surface thermal fronts (STFs) along the western Guangdong coast over the northern South China Sea shelf were analyzed using *in situ* observational data, remote sensing data, and numerical simulations. Both *in situ* and satellite observations show that the coastal thermal front exhibits substantial seasonal variability, being strongest in winter when it has the greatest extent and strongest sea surface temperature gradient. The winter coastal thermal front begins to appear in November and disappears after the following April. Although runoff water is more plentiful in summer, the front is weak in the western part of Guangdong. The frontal intensity has a significant positive correlation with the coastal wind speed, while the change of temperature gradient after September lags somewhat relative to the alongshore wind. The numerical simulation results accurately reflect the seasonal variation and annual cycle characteristics of the frontal structure in the simulated area. Based on vertical cross-section data, the different frontal lifecycles of the two sides of the Zhujiang (Pearl) River Estuary are analyzed.

Key words: oceanic thermal fronts, South China Sea, seasonal dynamics

Citation: Zhang Yan, Zeng Lili, Wang Qiang, Geng Bingxu, Liu Changjian, Shi Rui, Liu Na, Wang Weiping, Wang Dongxiao. 2021. Seasonal variation in the three-dimensional structures of coastal thermal front off western Guangdong. Acta Oceanologica Sinica, 40(7): 88–99, doi: 10.1007/s13131-021-1739-9

1 Introduction

An oceanic front is a typical mesoscale oceanic phenomenon identified by a discontinuity in, for example, temperature, salinity, or nutrient and chlorophyll *a* contents (Belkin et al., 2009). According to Yanagi and Koike (1987), oceanic fronts are classified into coastal water fronts, shelf fronts, and open ocean fronts. Numerous studies on the relationship between sea surface temperature (SST) and sea surface wind have been conducted on continental shelf and open ocean fronts in the equatorial and mid-latitude oceans. However, studies on the modification of the effect of sea surface wind on coastal water fronts have rarely been reported.

As an important physical process in the continental shelf, oceanic fronts play a vital role in the regional climate, carbon cycle, primary production, fisheries, coral bleaching, marine birds and mammals, and regional ecosystem (Simpson et al., 1978; D'Croz and Maté, 2004; Pauly and Christensen, 1995; Bost et al., 2009; Cabrera et al., 2011; Omand et al., 2015). The vigorous thermal fronts accompanied by high chlorophyll concentrations stretch several hundreds of kilometers along the shelf (Wang et al., 2001; Hu et al., 2003; Liu et al., 2010). Intense horizontal thermohaline gradients, enhanced turbulence, current shear, and surface convergence are closely linked with persistent fronts (Qiu et al., 2019). These dynamic processes contribute significantly to the high biological productivity in frontal zones (Johannessen et al., 2005; Holt and Umlauf, 2008; D'Asaro et al., 2011; Johnston et al., 2011; Long et al., 2012; Mahadevan et al., 2012; Omand et al., 2015).

The South China Sea (SCS) is an epi-continental marginal sea of the western Pacific Ocean, with a maximum depth of over 3 000 m (Liu et al., 2004). A main feature of its topography is a broad continental shelf shallower than 200 m (Fig. 1), linked to the deep basin by a steep shelf slope in the northern SCS (NSCS), where the isobaths are approximately parallel to the coastline. The climate and upper ocean circulation in the NSCS are dominated by the Asian monsoon, which blows northeasterly from October to April and southwesterly from May to September; spring and autumn are the monsoon transition periods (Xie et al., 2003). In response to monsoon forcing, the basin-scale circulation in the NSCS experiences an energetic seasonal cycle, which is generally cyclonic in winter and anticyclonic in summer (Hu et al., 2000; Liu et al., 2001; Su, 2004). Eddies with a range of hori-

Foundation item: The National Natural Science Foundation of China under contract Nos 41776025, 41576003, 41776026, 41676018 and 41806035; the Pearl River S&T Nova Program of Guangzhou under contract No. 201906010051; the Rising Star Foundation of the South China Sea Institute of Oceanology under contract No. NHXX2019WL0101; the Science and Technology Program of Guangzhou under contract No. 202002030490.

*Corresponding author, E-mail: wangweiping@smst.gz.cn

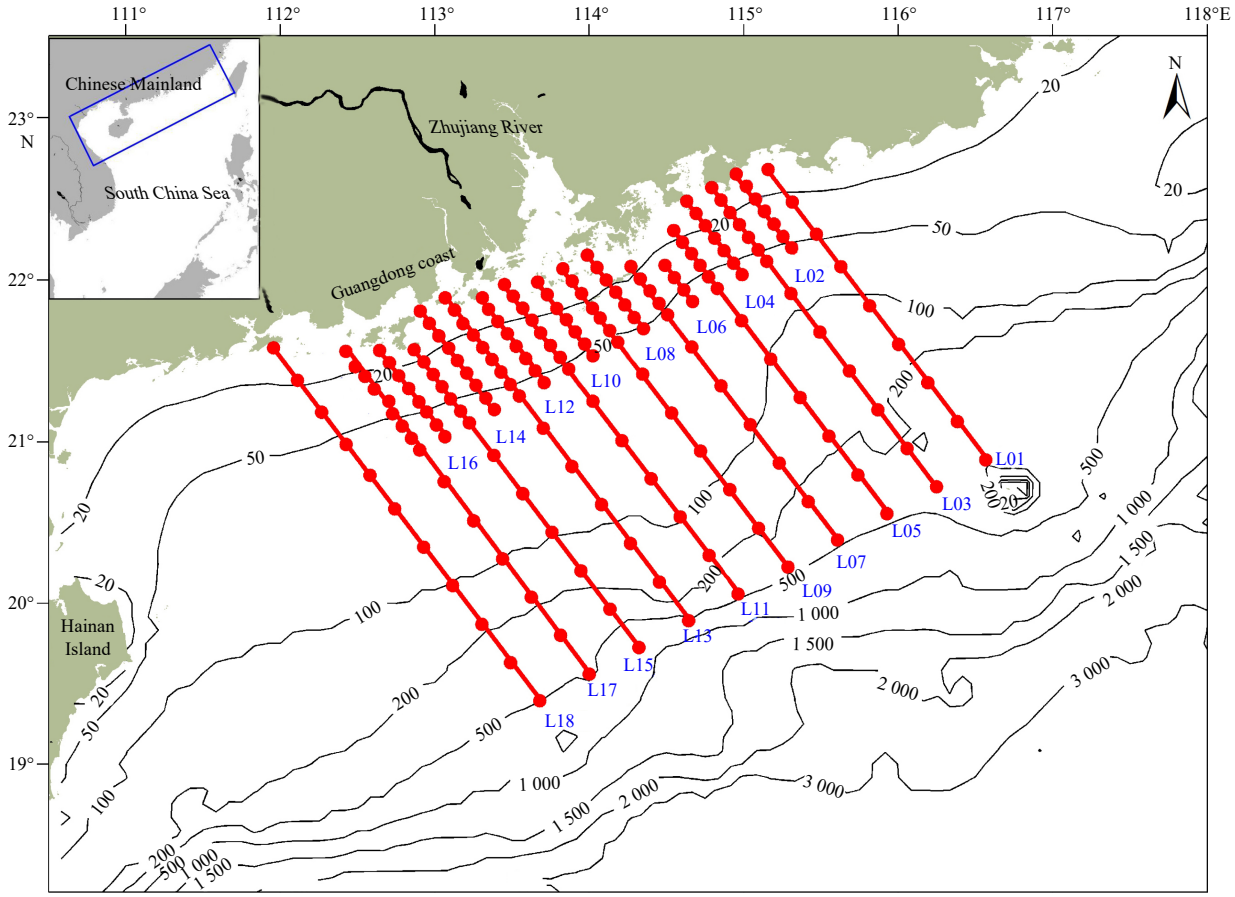

Fig. 1. Bathymetry (contours in m), *in situ* CTD stations (red dots). Four repeated cruise observations with 18 hydrographic transects along the cross-shelf red lines were implemented in summer (2006), winter (2006/2007), spring (2007), and autumn (2007), respectively. The blue box is the model area.

zontal scales are embedded in the circulation and they influence the shelf zone when they shift to continental slope (Su et al., 2020; Hwang and Chen, 2000; Wang et al., 2003; Chow et al., 2008; Nan et al., 2011). Driven by the persistent northeast monsoon in boreal winter, the net onshore Ekman transport over the broad continental shelf favors coastal downwelling and the development of vigorous STFs over the inner shelf (Gan et al., 2013). The winds reverse their direction and blow from the southwest in summer, triggering offshore Ekman transport of surface water over the shelf (Liu et al., 2001; Gan et al., 2009). As a result, persistent surface cooling and STFs are frequently observed in satellite SST during the summer upwelling season (e.g., Hu et al., 2003; Wang et al., 2014).

A wind-driven coastal current with an observed velocity of more than 0.2 m/s travels southwestward along the coast of the NSCS in winter, carrying cold water originating from higher latitudes. Thus, the cold coastal water transported by the coastal current, together with the shoreward accumulation of outer shelf warm water, also favors the development of winter STFs on the inner shelf. Although the position and intensity of these fronts change over time, the fronts tend to be approximately aligned with the shelf topography due to complex shelf dynamic processes that occur throughout the year.

Both the local fronts and coastal upwelling/downwelling have been widely documented in the NSCS by remote sensing measurements, field observations, and model outputs (e.g., Wang et al., 2001; Hu et al., 2003; Chang et al., 2006; Liu et al., 2010; Gan et al., 2013; Zhang et al., 2012). However, as common seasonal features under the influence of the monsoon regime, the shelf STFs in the NSCS and their underlying association with the seasonal wind forcing are not well understood to date, especially from the perspective of *in situ* observations at a sufficiently high spatial resolution. Results from field campaigns are important for understanding the formation mechanisms and variability of frontal activities in the NSCS.

There is a significant seasonal temporal and spatial variation of frontal activity over the shelf off the Zhujiang (Pearl) River Estuary. The seasonal mean of the temperature gradients calculated from satellite SST is highest in winter (Wang et al., 2001; Jing et al., 2016). During winter, the northeasterly monsoon causes strong cooling and stirring in the coastal sea and induces a southward intrusion of northern cold water along the coast (Shi et al., 2015). The results of comparison studies have shown that the STFs off the Zhujiang River Estuary are produced by the combined effect of the diluted fresh water from the Zhujiang River and the prevailing northeast monsoon, and are seen as an extension of the Fujian-Guangdong coastal front in the winter satellite SST gradient (Wang et al., 2012; Chang et al., 2006; Shi et al., 2015; Jing et al., 2016; Zhang et al., 2011). The variability of sea-surface thermal fronts is well studied use satellite data (Wang et al., 2001, 2004). But the three-dimensional structures, the detailed characteristics of these STFs and their underlying associations with the seasonal wind forcing have not been well understood in this region.

This study focuses on the three-dimensional structures and

seasonal variations of the STFs over the shelf off the Zhujiang River Estuary using four repeat field surveys, satellite measurements, and model simulations. Section 2 describes the *in situ* observations, the satellite-derived datasets, SST gradient calculation, and model simulations. The three-dimensional structures of seasonal STFs are investigated by *in situ* observations in Section 3. Section 4 discusses the relation between the thermal front and wind, and Section 5 presents the simulated seasonal variation and lifecycle of STFs. Finally, a summary is presented in Section 6.

2 Data and methods

2.1 *Shipboard hydrographic measurements*

A total of 4 repeat surveys, in summer and winter 2006 and spring and autumn 2007 (Table 1), were conducted over the shelf off the Zhujiang River Estuary in the NSCS (Fig. 1). The cruise tracks and positions of the CTD casts were designed to be the same in each survey, to obtain a better understanding of survey data by comparing these hydrographic structures in different seasons. On each cruise, there were 18 cross-shelf hydrographic transects covering the major front-development zones in the shelf off the Zhujiang River Estuary. The temperature, conductivity, and pressure were measured using a SeaBird 911 Plus CTD instrument.

Strict quality control was applied to the *in situ* data. In summer and autumn, the investigation was divided into several surveys because of typhoons and the onset of the winter monsoon, if the survey time slot was longer than 10 d in order to avoid calculation errors. The total number of CTDs and the selected CTDs used in this paper from the 4 surveys are listed in Table 1.

Table 1. Total number of CTDs and CTDs selected in this study from the 4 surveys

Cruise	Survey period	Total number of CTDs	Number of selected CTDs
Winter 2006/2007	Dec. 20, 2006–Jan. 20, 2007	234	234
Spring 2007	Apr. 6–May 4, 2007	233	233
Summer 2006	Jul. 14–Aug. 28, 2006	220	186
Autumn 2007	Oct. 9–Dec. 5, 2007	234	234

2.2 *Satellite remote sensing data*

The satellite remote sensing data used in this study include SST and sea surface wind from several satellite sensors. The SST data are derived from the operational SST and sea ice analysis (OSTIA) data provided by the Group for High Resolution SST (GHRSST) Pilot Project. This project was initiated by the Global Ocean Data Assimilation Experiment in 2000. OSTIA SST with a daily resolution of 0.05°×0.05° uses several types of satellite data from the GHRSST project, as well as *in situ* observations, to determine the SST for the global ocean. The OSTIA dataset provides robust data and acceptable near-shore accuracy, which enables it to identify coastal fronts in the NSCS. Among five sea surface temperature products based on satellite remote sensing observations, the OSTIA SST is considerable closer to the *in situ* observations. The OSTIA SST yields the smallest root mean square difference (RMSD) compared with independent buoy and ship observations in the coastal and shelf seas around China (Xie et al., 2008).

The sea surface wind data are from the quick scatterometer (QuikSCAT) and advanced scatterometer (ASCAT). QuikSCAT wind velocity is high-pass filtered using a 13-d running mean to examine the sea surface wind response at the synoptic time scale, which provides a more extensive geographical and temporal coverage and higher spatial resolution of ocean vector winds than those obtained by other space-borne sensors (Liu et al., 2002; Chelton and Wentz, 2005). Since QuikSCAT finished its mission in October 2009, ASCAT continues to provide global sea surface wind data.

The QuikSCAT data are distributed by Remote Sensing Systems (RSS) with a daily resolution of 0.25°×0.25°, and the ASCAT data from 2009 to 2016 are available from the Asia-Pacific Data Research Center. The existing data covering the NSCS frontal area are sufficient to support the present study despite the lack of near-shore data. The monthly climatological mean vector and scalar winds are calculated based on daily observations in this study and the wind data are based on 10-m equivalent neutral winds. Equivalent neutral wind is the wind that would exist under idealized conditions at a given height for a neutrally stratified atmospheric boundary layer.

2.3 *SST gradient calculation*

In this study, a gradient-based algorithm is utilized for each of the daily mean SST fields (Letelier et al., 2009). The intensity of the surface thermal front (STF) is quantitatively estimated by the SST gradient in each geo-referenced grid cell. The zonal and meridional components of the SST gradient ($GSST_X$, $GSST_Y$) are calculated via centered difference. The gradient magnitude (GM) is estimated by the following formula:

$$GM = \sqrt{(GSST_X)^2 + (GSST_Y)^2}. \quad (1)$$

2.4 *Model simulation*

We use the Regional Ocean Modeling System (ROMS) model, which covers the whole shelf and slope region of the NSCS (Fig. 1). This model uses a curvilinear horizontal orthogonal grid with an average spatial resolution of approximately 3 km, where the coordinate directions (x, y) are nearly aligned alongshore and cross-shore, respectively. There are 31 levels in the vertical.

The model uses SRTM30 topographic data (with a horizontal resolution of (1/30)°) (Farr and Kobrick, 2000) from the National Geophysical Data Center (NGDC, USA). The model was initialized using climatological temperature and salinity from the World Ocean Atlas 2013 and forced by 6-h CCMP wind (Atlas et al., 1996) and meteorological parameters from the National Centers for Environmental Prediction and National Center for Atmospheric Research (NCEP/NCAR). Hybrid Coordinate Ocean Model (HYCOM) reanalysis data (Bleck, 2002) for daily surface elevation, temperature, salinity, and currents are applied at the lateral open boundaries in the model. Eight tidal constituents (M_2, S_2, N_2, K_2, K_1, O_1, P_1 and Q_1) were used to calculate the hourly tidal elevation and currents using the results from the Oregon State University global tidal inverse model (Egbert and Erofeeva, 2002; Egbert et al., 1994). The daily river discharge of the Zhujiang River was obtained from the Zhujiang River Re-

sources Commission. After a spin-up period of 5 years with climatological winter-mean forcing, the model was run in hindcasting mode from 1 January 2000 to 1 December 2010. Daily output from 2000 to 2010 was used for analysis.

3 Observed thermal fronts

3.1 *Thermal fronts observed by the 4 in situ surveys*

Figure 2 presents the STFs observed from the 4 field campaigns in winter, spring, summer, and autumn of 2006–2007, respectively. Surface thermal front is obvious in winter and spring, and the maximum thermal gradients from *in situ* observation exceed 0.20°C/km.

Previous studies analyzed the thermal fronts outside the Zhujiang River Estuary as a single entity in winter (Wang et al., 2001; Shi et al., 2015; Jing et al., 2016), but the *in situ* results show that the front located around the Zhujiang River Estuary is not a simple response to a single mechanism as previously studied (SCSB/SOA, 1990), but should be separated into two parts for analysis (Fig. 2).

The *in situ* SST gradient in Fig. 2 shows that in winter the STFs on the west side of the Zhujiang River Estuary are clearly induced by the colder fresher water from the Zhujiang River. The strong northeast wind drives the runoff water southwest along the coast and the front forms at the head of the estuary, although the runoff from the Zhujiang River reaches a minimum during winter. On the east side of the Zhujiang River Estuary the STFs merge with the front to the northeast but are located farther offshore; the front to the northeast is formed where southward-moving Fujian coastal cold water from northwestern Fujian meets the warm water ahead.

Spring is the transition season of the monsoon regime, when the northeast winds weaken gradually and are eventually replaced by the reverse summer monsoon winds at the end of spring (Wang et al., 2012). The wind direction is nearly east during the spring survey and the intensity clearly decreases. The STFs off the western part of the Zhujiang River Estuary persist although their extent is reduced slightly, but the STFs off the eastern part of the Zhujiang River Estuary almost disappear. In winter and spring, the patterns of the salinity front on the west side of the Zhujiang River Estuary are almost the same as those of the thermal front, so the thermal front in this region is mainly formed by the influence of Zhujiang River water in these two seasons.

In summer, the front around the Zhujiang River Estuary disappears as a result of the prevailing southwest monsoon, and the cross-shelf thermohaline structures in the vertical profiles are dominated by coastal upwelling and topographic effects (Gan et al., 2009; Su and Pohlmann, 2009). The *in situ* measured SST gradient in summer does not show a notable Zhujiang River plume front. In the summer survey the STFs were located mostly at the boundary of Guangdong Province where upwelling frequently occurs; STFs are found where cold water from the deep

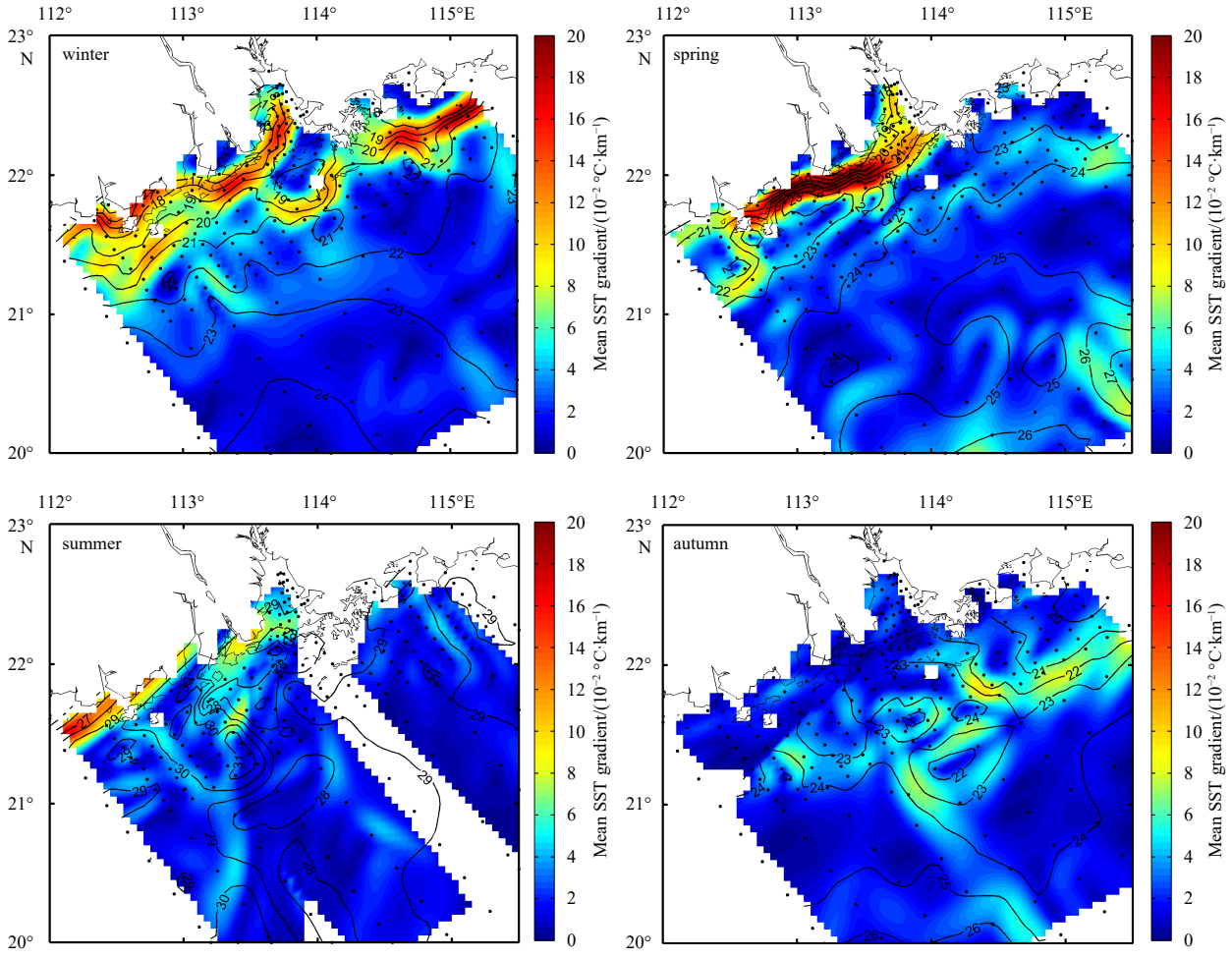

Fig. 2. Seasonal mean SST gradients (shading) and SST (contours in°C) *in situ* in the northern South China Sea.

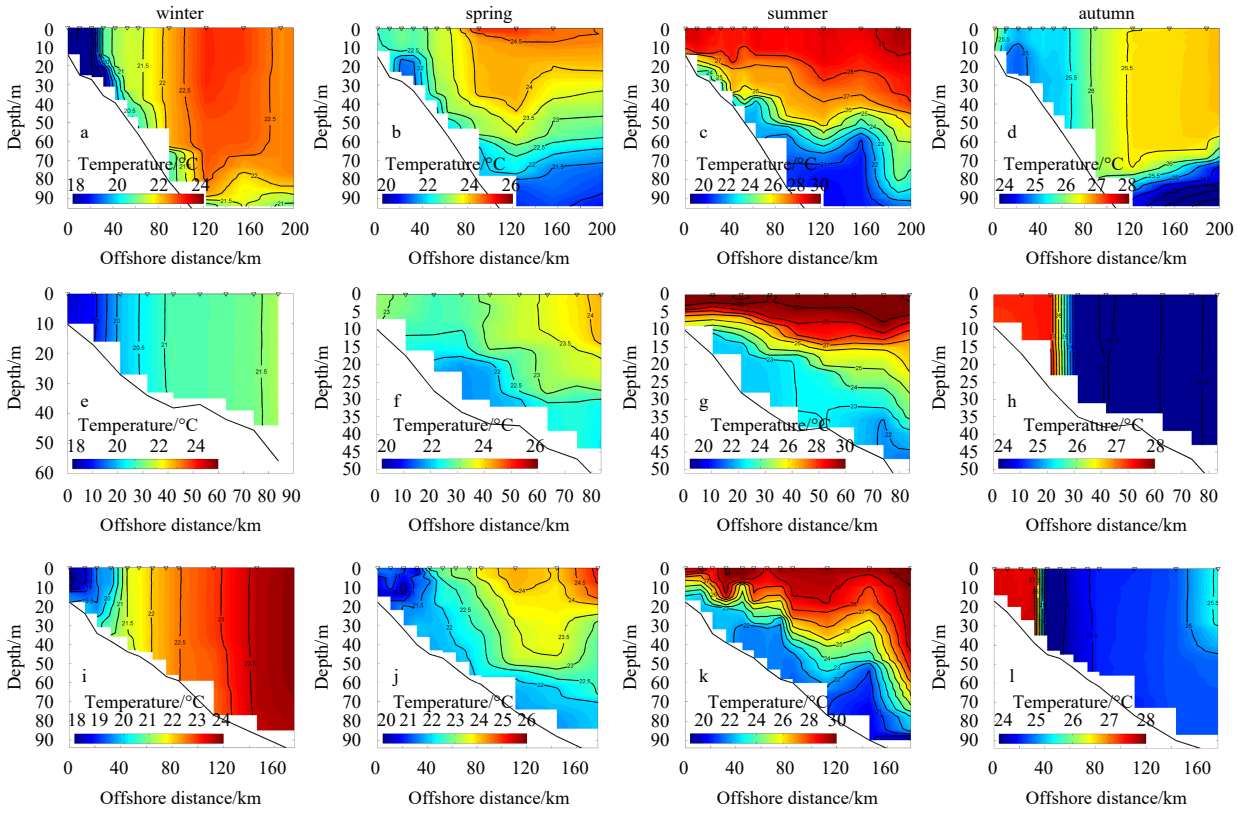

Fig. 3. Vertical structures of *in situ* temperature in the representative cross-shelf transects L03 (a–d), L14 (e–h) and L17 (i–l) in four seasons.

layers upwells, as is seen more clearly in the vertical profiles (Fig. 3).

In autumn the opposite transition occurs, from southwest to northeast prevailing wind. Most stations of the autumn survey were sampled in November after the onset of the winter monsoon, when the front on the west side of the Zhujiang River Estuary had not yet formed. On the east side of the Zhujiang River Estuary the thermal front had started to appear with a similar pattern to that in winter. These results show that wind forcing plays an important role in the seasonal cycle of thermal front activity.

3.2 *Cross-shelf vertical structures of seasonal thermal fronts*

To identify the differences in thermal fronts between the western and eastern parts of the Zhujiang River Estuary, we select three sections that cover the two sides (L03 in the east; L14 and L17 in the west) of the estuary.

In winter, water in the upper layer is well mixed with a mixed layer depth of 70 m (L03); at depths less than 70 m in the profile the vertical thermal (Fig. 3) and salinity structures have nearly the same pattern. The L03 profile shows an obvious thermohaline front with sharp thermal and salinity gradients from the sea surface to the bottom (Yanagi and Koike, 1987). On the cross-shelf transect the main body of the thermohaline front occurs between 20 m and 50 m depth, and corresponds to the strong band-shaped thermal fronts on the shelf over the eastern side of the Zhujiang River Estuary in winter. In spring, as the mixed layer depth is reduced, the thermohaline front weakens and nearly disappears. In summer, the thermohaline front disappears in the L03 section and there is evident upwelling. In autumn, as the northeast prevailing wind strengthens, the upper layer is well mixed and the thermohaline front appears, although the intensity is weaker than in winter.

The L14 and L17 sections are both on the western side of the Zhujiang River Estuary. Temperature and salinity profiles show a thermohaline front in winter and autumn. The offshore gradient of sea temperature in L17 is stronger than in L14 during winter and spring, although L17 is farther from the Zhujiang River Estuary. This phenomenon can be found more clearly in the salinity profiles, and may be due to the strong northeasterly winter monsoon wind forcing. In summer, the gradient of temperature in the x direction disappears, and the L14 salinity gradient strengthens greatly, becoming stronger than that in L17 under the influence of plentiful diluted Zhujiang River water and the southwest wind that traps the diluted water. In autumn the situation is similar to that in winter, but the gradients of temperature and salinity are slightly weaker.

3.3 *Probability of occurrence of surface thermal fronts, as inferred from satellite data*

The probabilities of occurrence of STFs in each month are calculated from the daily SST dataset from 2006 to 2015. In the calculation, only STFs with local temperature gradients greater than 0.03°C/km were retained. Areas with a probability of developing STFs greater than 30% are consistent with the spatial patterns of frontal intensities at the sea surface observed from satellite data (Fig. 4). The monthly climatological winds are shown in Fig. 5. In November, forcing by the strong northeast winter monsoon results in sea water that is being brought onto the shelf by Ekman drift piling up in the northwestern part of the SCS and the thermal front appears as a strong band-shaped area with a high probability of front occurrence that persists throughout the winter.

The probability of thermal front occurrence reaches its max-

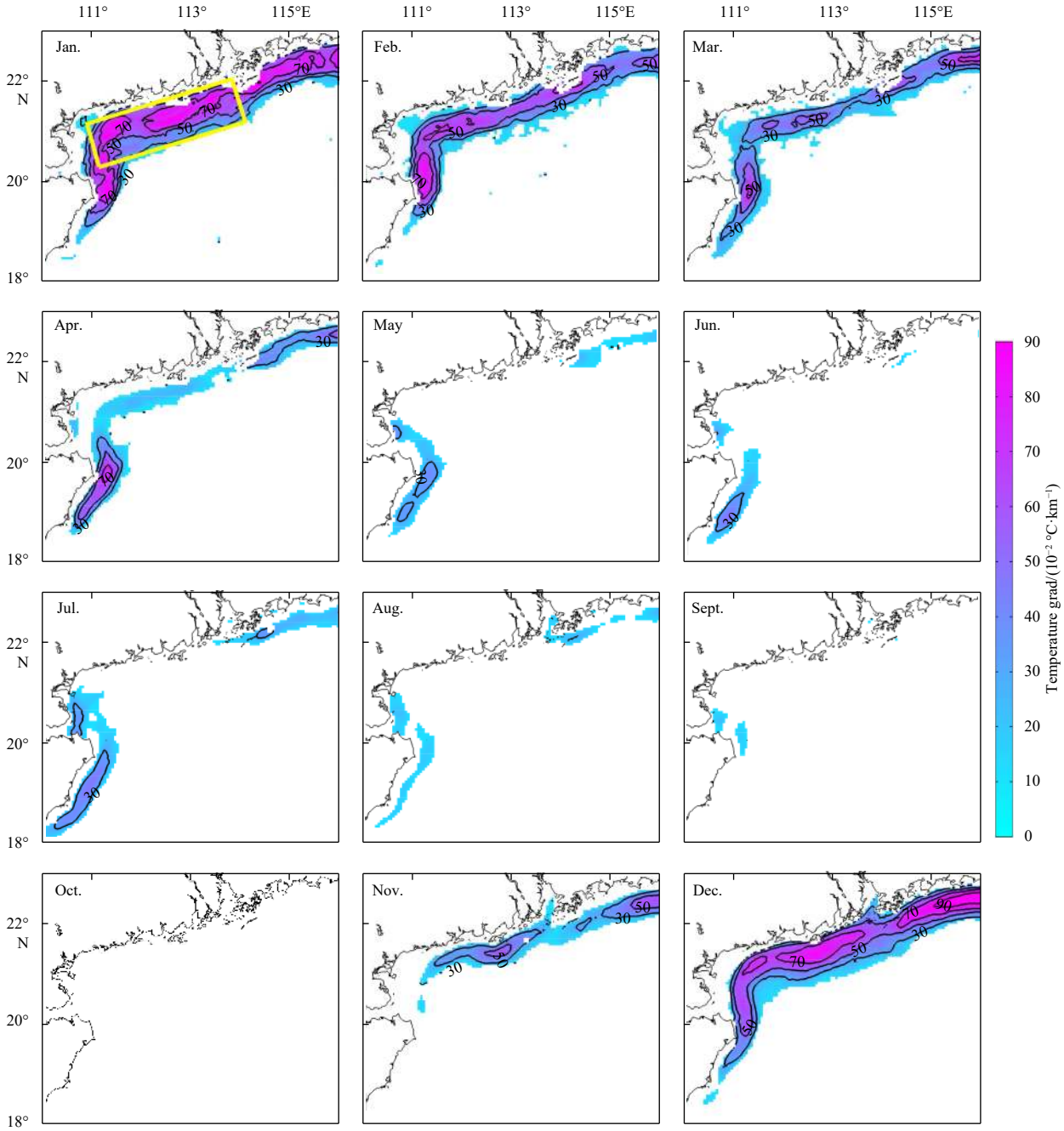

Fig. 4. Monthly climatological variations in probability of thermal front occurrence in the NSCS. The probabilities are calculated from satellite-derived OSTIA daily SST data for 2006–2014 with temperature gradients greater than 0.03°C/km. The yellow box is the regional-mean area.

imum in January, over the 100 km nearest the coast on both sides of the Zhujiang River Estuary. Off the western side of the estuary the thermal front is present from November to the following February, decays from February to May, and disappears from June to October. The STFs have a high probability of occurrence in the winter half year (November–April) but nearly disappear in the summer half year (May–October).

4 Relation between thermal front and wind

As the occurrence of STFs in each month generally has some connection with the wind forcing (see Section 2.2), we choose a box region (shown in Fig. 4) to study the relation between them using a regional-mean time series (Fig. 6).

The regional-mean front index over the western shelf of the Zhujiang River Estuary reaches its maximum value in January and minimum in September. Except in summer when the offshore wind is weak, the variation of the front index is consistent with the seasonal cycle of alongshore wind, but lags a little after September. The direction of_the wind perpendicular to the coast determines the variation of the thermal gradient; offshore wind velocity has a positive correlation with thermal gradient, and onshore wind velocity has a negative correlation with thermal gradient. This suggests that the frontal activity is closely related to the seasonal wind forcing in this region.

Fig. 5. Monthly climatological surface wind in the NSCS.

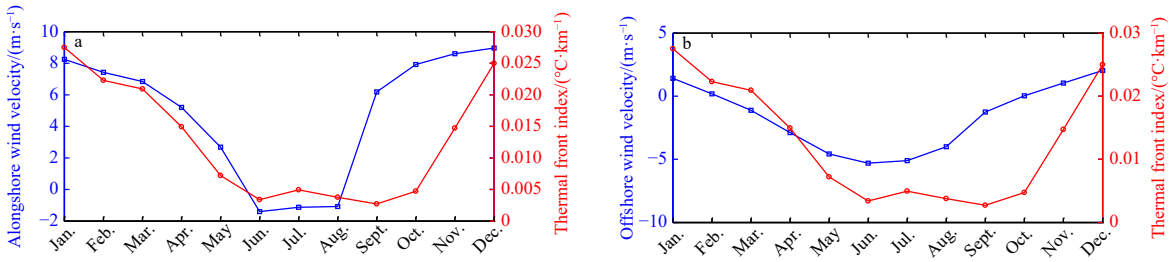

Fig. 6. Seasonal cycles of alongshore (a) and offshore (b) wind speed (blue) and thermal front index (red) averaged over the shelf (yellow dashed box shown in Fig. 4). The thermal front index is defined as the intensity of the surface thermal front multiplied by the probability of front occurrence. The time series are all normalized by their respective root-mean-square variance.

5 Simulated seasonal variation and lifecycle of STFs

In situ surveys are limited because they are time-consuming and expensive. Satellite data measurements can only reflect the characteristics of the sea surface, although the spatial patterns of STFs are almost same to the *in situ* results, but the values are weakened by quality control methods, such as interpolation and assimilation (Fig. 7). Here, the ROMS model is used to further examine the thermodynamic mechanisms of the coastal front. The numerical simulation results accurately reflect the seasonal variation and annual cycle of the front structures in the simulated

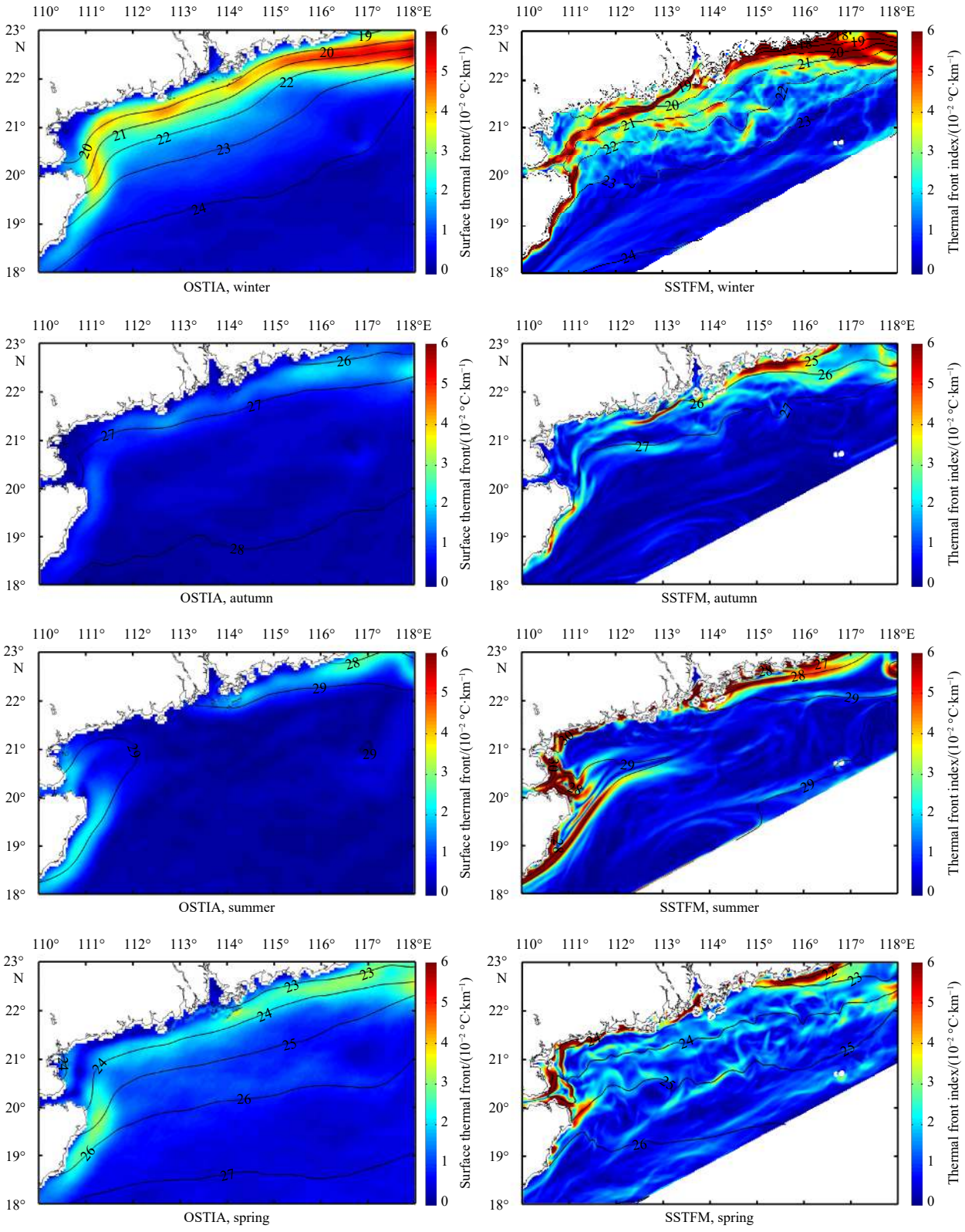

Fig. 7. The satellite-derived (left) surface thermal fronts (shading) and SST (contours in °C), and model simulation (right) surface thermal fronts (shading) and SST (contours in °C).

area. Vertical cross-sections are used to analyze the different frontal lifecycles on the two sides of the Zhujiang River Estuary.

The results of the numerical simulation (Fig. 7) show that the seasonal variation in the simulated area is consistent with that seen from satellite observations, and the distribution of the fronts across the four seasons is simulated well, especially the reappearance of the thermal front pattern in winter. The strength of the front is stronger than in satellite observations, and is close to the value of *in situ* observations. We analyze the annual cycle of the Zhujiang River Estuary coastal STFs with the simulated results for the L03 and L17 profiles.

The L03 profile is on the east of the Zhujiang River Estuary, an area strongly influenced by the winter monsoon and the southward movement of the Fujian coastal cold water in winter. The modeled temperature distribution along the L03 profile (Fig. 8) shows that along the coast where the depth is about 30 m the thermal front is significant with a sharp temperature gradient in winter (December, January, February); the front extends across the whole vertical profile from the surface to the bottom, which is consistent with the *in situ* observations (Fig. 3), and then weakens in March and disappears in April and May. In June, under the influence of upwelling the thermal front appears off the coast at depths of 10–50 m; its strength and range are greater than the thermal front in winter, and it develops and strengthens in July and August, before weakening and disappearing in September. However, this is not seen in the satellite observations because the front occurs below the sea surface. In October, the temperature gradient seems to strengthen in the region of the winter front, and the winter thermal front is formed in November.

The modelled thermal front lifecycle of the L17 profile (Fig. 9) is similar to that of L03. The coastal thermal front is significant in winter, and the thermal front induced by upwelling develops in summer, but with weaker intensity than the thermal front of L03.

6 Summary

In this study, seasonal variation in the three-dimensional structures and the lifecycle of the shelf STFs on the coast of the NSCS are investigated, with satellite data and 4 repeat fine-resol-

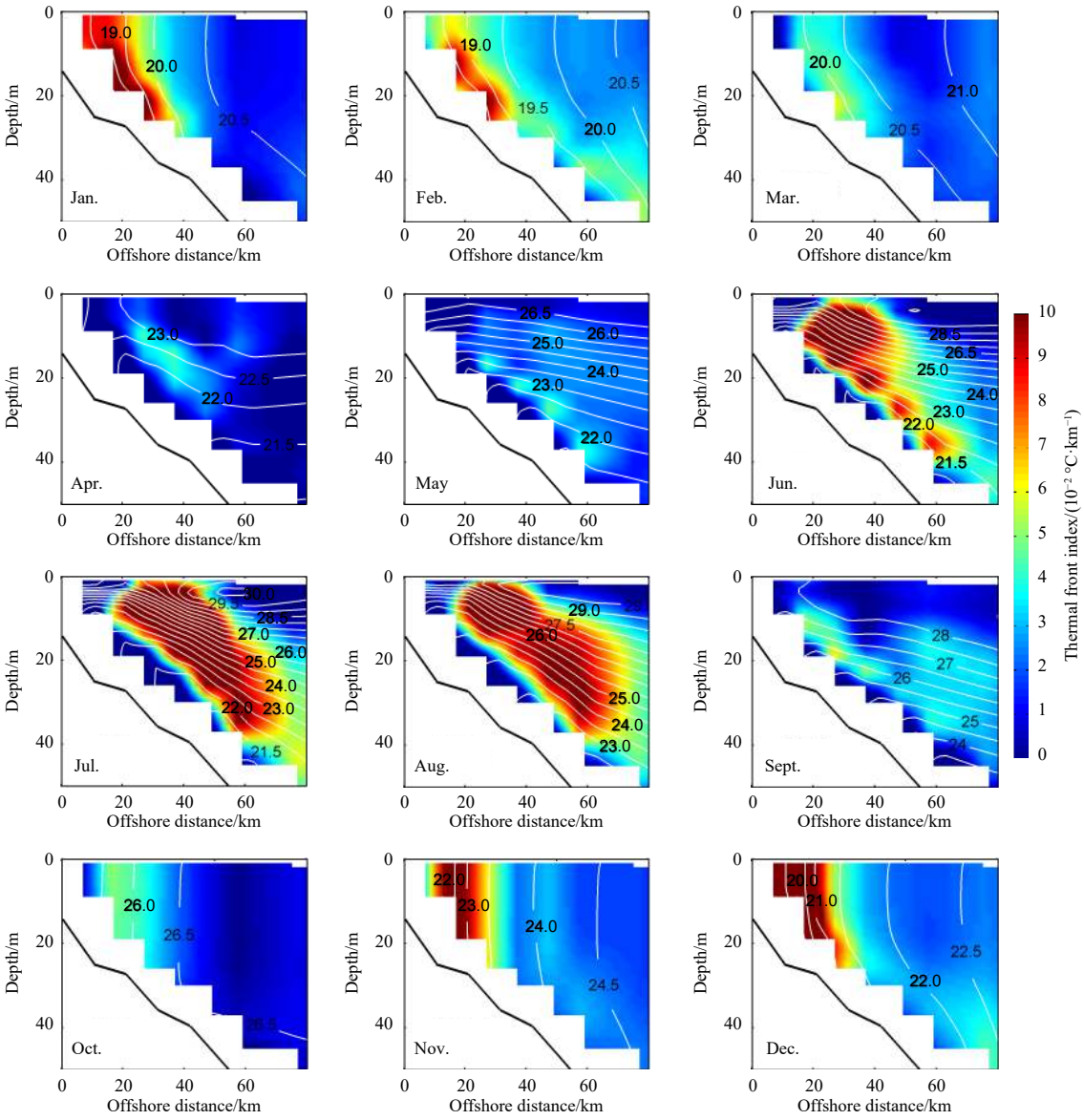

Fig. 8. Model simulation results for the thermal front lifecycle for the L03 profile. Thermal fronts: shading, and temperature: contours in °C.

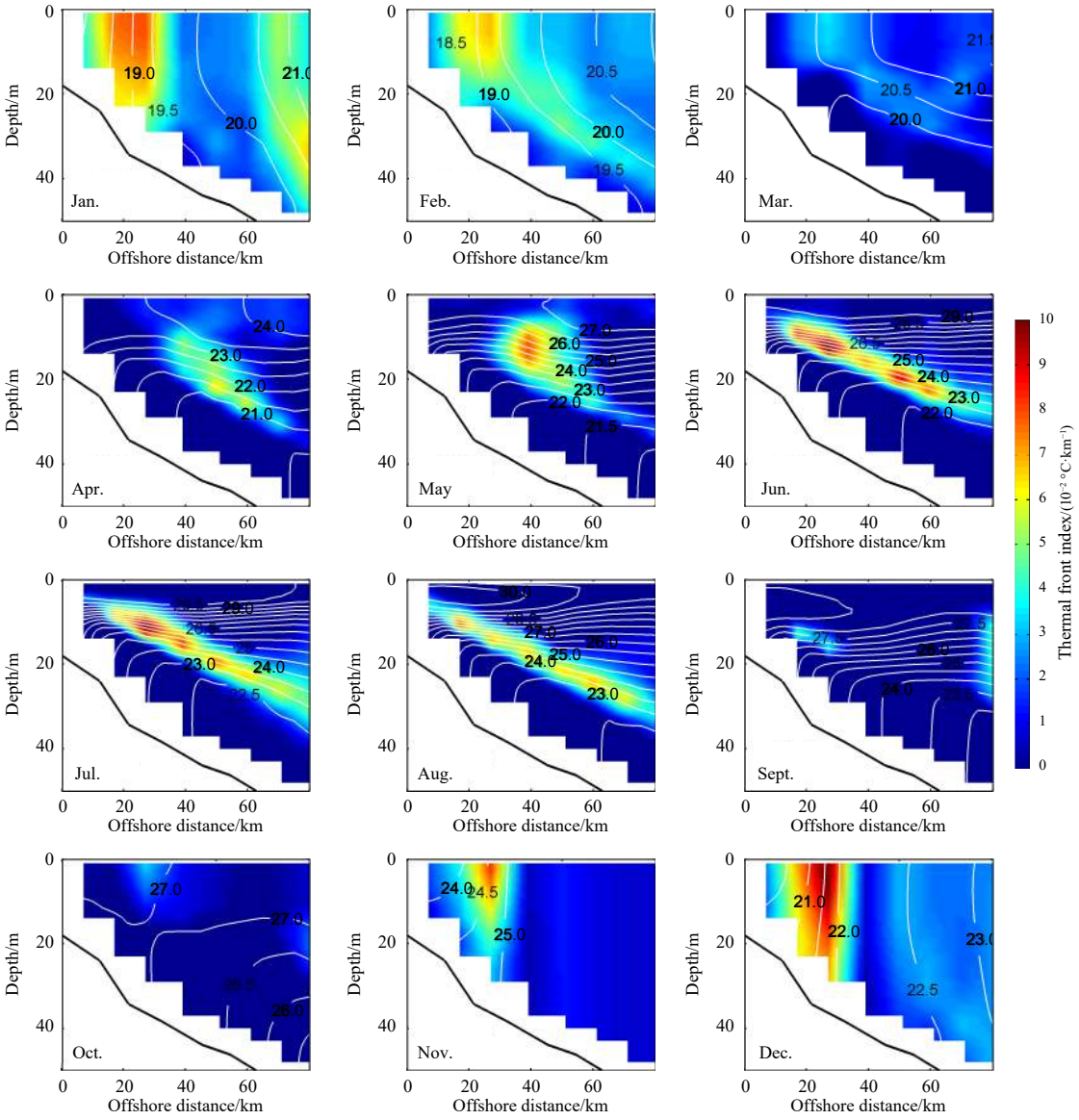

Fig. 9. Model simulation results for the thermal front lifecycle for the L17 profile. Thermal fronts: shading, and temperature: contours in °C.

ution *in situ* surveys in four seasons of 2006–2007. A model is used to further examine the lifecycle and thermodynamic mechanisms of the coastal front and their underlying associations with wind forcing.

Both *in situ* and satellite observations show that the coastal thermal front exhibits substantial seasonal variability. The front is strongest and has its greatest extent and strongest sea surface temperature gradient in winter. The *in situ* data show that the front located around the Zhujiang River Estuary is not a simple response to a single mechanism as previously studied, but that it should be considered as two separate parts. In winter, the STFs on the west side of the Zhujiang River Estuary are induced by the colder diluted freshwater from the Zhujiang River, and on the east side of the Zhujiang River Estuary the STFs merge with the front to the northeast but are located farther offshore; the front to the northeast is formed where southward-moving Fujian coastal cold water from northwestern Fujian meets the warm water ahead. In spring, there are still STFs over the western part of the Zhujiang River Estuary, although they cover a smaller area, but the STFs over the eastern part of the Zhujiang River Estuary almost disappear. In summer, the front around the Zhujiang River Estuary disappears, and the SST gradient of *in situ* observations, driven by the prevailing southwest monsoon, does not show a notable Zhujiang River plume front. In autumn, there is still no front in the western part of the Zhujiang River Estuary, but in the eastern part of the estuary the thermal front begins to reappear with a similar pattern to that in winter.

The results from both field campaigns and satellite measurements suggest that the seasonal wind forcing plays an important role in determining the frontal activity over the shelf. The ROMS model is used to further examine the thermodynamic mechanisms driving the coastal front. The numerical simulation results accurately reflect the seasonal variation and annual cycle characteristics of the front structure in the L03 and L17 profiles, and show the differences in frontal lifecycle between the two sides of the Zhujiang River Estuary.

References

Atlas R, Hoffman R N, Bloom S C, et al. 1996. A multiyear global surface wind velocity dataset using SSM/I wind observations. Bulletin of the American Meteorological Society, 77(5): 869–882, doi: 10.1175/1520-0477(1996)077<0869:AMGSWV>2.0.CO;2

Belkin I M, Cornillon P C, Sherman K. 2009. Fronts in large marine ecosystems. Progress in Oceanography, 81(1–4): 223–236

Bleck R. 2002. An oceanic general circulation model framed in hybrid isopycnic-Cartesian coordinates. Ocean Modelling, 4(1): 55–88, doi: 10.1016/S1463-5003(01)00012-9

Bost C A, Cotté C, Bailleul F, et al. 2009. The importance of oceanographic fronts to marine birds and mammals of the southern oceans. Journal of Marine Systems, 78(3): 363–376, doi: 10.1016/j.jmarsys.2008.11.022

Cabrera O C, Villanoy C L, David L T, et al. 2011. Barrier layer control of entrainment and upwelling in the Bohol Sea, Philippines. Oceanography, 24(1): 130–141, doi: 10.5670/oceanog.2011.10

Chang Y, Shimada T, Lee M A, et al. 2006. Wintertime sea surface temperature fronts in the Taiwan Strait. Geophysical Research Letters, 33(23): L23603, doi: 10.1029/2006GL027415

Chelton D B, Wentz F J. 2005. Global microwave satellite observations of sea surface temperature for numerical weather prediction and climate research. Bulletin of the American Meteorological Society, 86(8): 1097–1116, doi: 10.1175/BAMS-86-8-1097

Chow C H, Hu J H, Centurioni L R, et al. 2008. Mesoscale Dongsha cyclonic eddy in the northern South China Sea by drifter and satellite observations. Journal of Geophysical Research: Oceans, 113(C4): C04018, doi: 10.1029/2007JC004542

D'Asaro E, Lee C, Rainville L, et al. 2011. Enhanced turbulence and energy dissipation at ocean fronts. Science, 332(6027): 318–322, doi: 10.1126/science.1201515

D'Croz L, Maté J L. 2004. Experimental responses to elevated water temperature in genotypes of the reef coral *Pocillopora damicornis* from upwelling and non-upwelling environments in Panama. Coral Reefs, 23(4): 473–483, doi: 10.1007/s00338-004-0397-7

Egbert G D, Bennett A F, Foreman M G G. 1994. TOPEX/Poseidon tides estimated using a global inverse model. Journal of Geophysical Research: Oceans, 99(C12): 24821–24852, doi: 10.1029/94JC01894

Egbert G D, Erofeeva S Y. 2002. Efficient inverse modeling of barotropic ocean tides. Journal of Atmospheric and Oceanic Technology, 19(2): 183–204, doi: 10.1175/1520-0426(2002)019<0183:EIMOBO>2.0.CO;2

Farr T G, Kobrick M. 2000. Shuttle radar topography mission produces a wealth of data. EOS, 81(48): 583–585, doi: 10.1029/EO081i048p00583

Gan Jianping, Cheung A, Guo Xiaogang, et al. 2009. Intensified upwelling over a widened shelf in the northeastern South China Sea. Journal of Geophysical Research: Oceans, 114(C9): C09019, doi: 10.1029/2007JC004660

Gan Jianping, Ho H S, Liang Linlin. 2013. Dynamics of intensified downwelling circulation over a widened shelf in the northeastern South China Sea. Journal of Physical Oceanography, 43(1): 80–94, doi: 10.1175/JPO-D-12-02.1

Holt J, Umlauf L. 2008. Modelling the tidal mixing fronts and seasonal stratification of the Northwest European Continental shelf. Continental Shelf Research, 28(7): 887–903, doi: 10.1016/j.csr.2008.01.012

Hu Jianyu, Kawamura H, Hong Huasheng, et al. 2000. A review on the currents in the South China Sea: Seasonal circulation, South China Sea warm current and Kuroshio intrusion. Journal of Oceanography, 56(6): 607–624, doi: 10.1023/A:1011117531252

Hu Jianyu, Kawamura H, Tang D L. 2003. Tidal front around the Hainan Island, northwest of the South China Sea. Journal of Geophysical Research: Oceans, 108(C11): 3342, doi: 10.1029/2003JC001883

Hwang C, Chen S A. 2000. Circulations and eddies over the South China Sea derived from TOPEX/Poseidon altimetry. Journal of Geophysical Research: Oceans, 105(C10): 23943–23965, doi: 10.1029/2000JC900092

Jing Zhiyou, Qi Yiquan, Fox-Kemper B, et al. 2016. Seasonal thermal fronts on the northern South China Sea shelf: Satellite measurements and three repeated field surveys. Journal of Geophysical Research: Oceans, 121(3): 1914–1930, doi: 10.1002/2015JC011222

Johannessen J A, Kudryavtsev V, Akimov D, et al. 2005. On radar imaging of current features: 2. Mesoscale eddy and current front detection. Journal of Geophysical Research: Oceans, 110(C7): C07017, doi: 10.1029/2004JC002802

Johnston T M S, Rudnick D L, Pallàs-Sanz E. 2011. Elevated mixing at a front. Journal of Geophysical Research: Oceans, 116(C11): C11033, doi: 10.1029/2011JC007192

Letelier J, Pizarro O, Nuñez S. 2009. Seasonal variability of coastal upwelling and the upwelling front off central Chile. Journal of Geophysical Research: Oceans, 114(C12): C12009, doi: 10.1029/2008JC005171

Liu W T. 2002. Progress in scatterometer application. Journal of Oceanography, 58(1): 121–136, doi: 10.1023/A:1015832919110

Liu Sumei, Guo Xinyu, Chen Qi, et al. 2010. Nutrient dynamics in the winter thermohaline frontal zone of the northern shelf region of the South China Sea. Journal of Geophysical Research: Atmospheres, 115(C11): C11020, doi: 10.1029/2009JC005951

Liu Qinyu, Jiang Xia, Xie S P, et al. 2004. A gap in the Indo-Pacific warm pool over the South China Sea in boreal winter: Seasonal development and interannual variability. Journal of Geophysical Research: Oceans, 109(C7): C07012, doi: 10.1029/2003JC002179

Liu Zhengyu, Yang Haijun, Liu Qinyu, et al. 2001. Regional dynamics of seasonal variability in the South China Sea. Journal of Physical Oceanography, 31: 272–284, doi: 10.1175/1520-0485(2001)031<0272:RDOSVI>2.0.CO;2

Long M C, Thomas L N, Dunbar R B. 2012. Control of phytoplankton bloom inception in the Ross Sea, Antarctica, by Ekman restratification. Global Biogeochemical Cycles, 26(1): GB1006, doi: 10.1029/2010GB003982

Mahadevan A, D'Asaro E, Lee C, et al. 2012. Eddy-driven stratification initiates North Atlantic spring phytoplankton blooms. Science, 337(6090): 54–58, doi: 10.1126/science.1218740

Nan Feng, He Zhigang, Zhou Hui, et al. 2011. Three long-lived anticyclonic eddies in the northern South China Sea. Journal of Geophysical Research: Oceans, 116(C5): C05002, doi: 10.1029/2010JC006790

Omand M M, D'Asaro E A, Lee C M, et al. 2015. Eddy-driven subduction exports particulate organic carbon from the spring bloom. Science, 348(6231): 222–225, doi: 10.1126/science.1260062

Pauly D, Christensen V. 1995. Primary production required to sustain global fisheries. Nature, 374(6519): 255–257, doi: 10.1038/374255a0

Qiu Chunhua, Mao Huabin, Liu Hailong, et al. 2019. Deformation of a warm eddy in the northern South China Sea. Journal of Geophysical Research: Oceans, 124(8): 5551–5564, doi: 10.1029/2019JC015288

Shi Rui, Guo Xinyu, Wang Dongxiao, et al. 2015. Seasonal variability in coastal fronts and its influence on sea surface wind in the Northern South China Sea. Deep Sea Research Part II: Topical Studies in Oceanography, 119: 30–39, doi: 10.1016/j.dsr2.2013.12.018

Simpson J H, Allen C M, Morris N C G. 1978. Fronts on the continental shelf. Journal of Geophysical Research: Oceans, 83(C9): 4607–4614, doi: 10.1029/JC083iC09p04607

South China Sea Branch of State Ocean Administration of China (SCSB/SOA). 1990. Report on Decadal Hydrographic Investigation in the sea areas adjacent to the shelf of the northern South China Sea (in Chinese). Beijing: China Ocean Press, 42–93

Su Jilan. 2004. Overview of the South China Sea circulation and its influence on the coastal physical oceanography outside the Pearl River Estuary. Continental Shelf Research, 24(16): 1745–1760, doi: 10.1016/j.csr.2004.06.005

Su Danyi, Lin Pengfei, Mao Huabin, et al. 2020. Features of slope intrusion mesoscale eddies in the northern South China Sea. Journal of Geophysical Research: Oceans, 125(2): e2019JC015349, doi:

10.1029/2019JC015349

Su Jian, Pohlmann T. 2009. Wind and topography influence on an upwelling system at the eastern Hainan coast. Journal of Geophysical Research: Oceans, 114(C6): C06017, doi: 10.1029/2008JC005018

Wang Guihua, Li Jiaxun, Wang Chunzai, et al. 2012. Interactions among the winter monsoon, ocean eddy and ocean thermal front in the South China Sea. Journal of Geophysical Research: Oceans, 117(C8): C08002, doi: 10.1029/2012JC008007

Wang Dongxiao, Liu Yun, Qi Yiquan, et al. 2001. Seasonal variability of thermal fronts in the northern South China Sea from satellite data. Geophysical Research Letters, 28(20): 3963–3966, doi: 10.1029/2001GL013306

Wang Dongxiao, Shu Yeqiang, Xue Huijie, et al. 2014. Relative contributions of local wind and topography to the coastal upwelling intensity in the northern South China Sea. Journal of Geophysical Research Oceans: Oceans, 119(4): 2550–2567, doi: 10.1002/2013JC009172

Wang Guihua, Su Jilan, Chu P C. 2003. Mesoscale eddies in the South China Sea observed with altimeter data. Geophysical Research Letters, 30(21): 2121, doi: 10.1029/2003GL018532

Wang Lei, Wong Liya, Wei Hao. 2004. An analysis of the sea-surface thermal fronts in the northern shelf region of the South China Sea with satellite data. Periodical of Ocean University of China (in Chinese), 34(3): 351–357

Xie S-P, Xie Qiang, Wang Dongxiao, et al. 2003. Summer upwelling in the South China Sea and its role in regional climate variations. Journal of Geophysical Research: Oceans, 108(C8): 3261, doi: 10.1029/2003JC001867

Xie Jiping, Zhu Jiang, Li Yan. 2008. Assessment and inter-comparison of five high-resolution sea surface temperature products in the shelf and coastal seas around China. Continental Shelf Research, 28(10–11): 1286–1293

Yanagi T, Koike T. 1987. Seasonal variation in thermohaline and tidal fronts, Seto Inland Sea, Japan. Continental Shelf Research, 7(2): 149–160, doi: 10.1016/0278-4343(87)90076-8

Zhang Yan, Wang Dongxiao, Xia Huayong, et al. 2012. The seasonal variability of an air-sea heat flux in the northern South China Sea. Acta Oceanologica Sinica, 31(5): 79–86, doi: 10.1007/s13131-012-0238-4

Zhang Yan, Xia Huayong, Qian Libing, et al. 2011. Analysis on hydrological characteristics off the Pearl River Estuary in summer and winter of 2006. Journal of Tropical Oceanography (in Chinese), 30(1): 20–28